

Wavelet analysis of magnetic turbulence in the Earth's plasma sheet

Z. Vörös,* W. Baumjohann, R. Nakamura, A. Runov, M. Volwerk,[†] and T.L. Zhang

Space Research Institute, Austrian Academy of Sciences, Graz, Austria

A. Balogh

Imperial College, London, UK

(Dated: October 7, 2018)

Abstract

Recent studies provide evidence for the multi-scale nature of magnetic turbulence in the plasma sheet. Wavelet methods represent modern time series analysis techniques suitable for the description of statistical characteristics of multi-scale turbulence. Cluster FGM (fluxgate magnetometer) magnetic field high-resolution (67 Hz) measurements are studied during an interval in which the spacecraft are in the plasma sheet. As Cluster passes through different plasma regions, physical processes exhibit non-steady properties on magnetohydrodynamic (MHD) and small, possibly kinetic scales. As a consequence, the implementation of wavelet-based techniques becomes complicated due to the statistically transitory properties of magnetic fluctuations and finite size effects. Using a supervised multi-scale technique which allows existence test of moments, the robustness of higher-order statistics is investigated. On this basis the properties of magnetic turbulence are investigated for changing thickness of the plasma sheet.

*Electronic address: zoltan.voeroes@oeaw.ac.at

[†]Also at Max-Planck Institute for Extraterrestrial Physics, Garching, Germany

I. INTRODUCTION

Direct observations of the velocity and magnetic field in the plasma sheet have revealed strong intermittent fluctuations in the temporal and spatial domains. These observations were attributed to turbulence [1]. Eddy turbulence rather than Alfvénic turbulence seems to prevail and the most important dissipation mechanisms include a multi-scale cascade of energy to non-magnetohydrodynamic (non-MHD) scales and an electrical coupling of the turbulent flows to the ionosphere [2]. In contrast with the classical hydrodynamic or MHD homogeneous turbulence picture [3, 4], MHD turbulence in the plasma sheet is not free from boundary effects [2, 5]. Moreover, due to the movement of boundaries (e.g. the plasma sheet boundary layer (PSBL), or a flow channel built up during rapid plasma flows) and the transitory character of driving mechanisms (e.g. shear flows, sporadic reconnection, MHD instabilities), the observed processes show intermittence in time rather than intermittence in space, an important clue for distinguishing homogeneous and non-homogeneous plasma sheet flows [6]. Intermittence is related to long-tailed probability distributions, hence to higher order statistical moments. In general, statistical moments are defined by the average of the powers of a random variable. In solar wind intermittence studies it is customary to use q -th order absolute powers of velocity, magnetic field, etc. increments (so-called q -th order structure functions) [7, 8], which allow to investigate the multi-scale scaling features of fluctuations with long-tailed probability distributions. Direct studies of empirical probability densities of increment fields in the solar wind revealed departures from a Gaussian distribution over multiple scales [9] and an increase of intermittence towards small scales [10]. Another class of intermittence studies uses large deviation concepts reconstructing distribution functions of burstiness of local fluctuations in considered fields [6, 11]. An alternative for studying multi-scale space plasma intermittence is represented by the wavelet method [12, 13], which also proved to be useful in resolving multi-scale cascading features of a current disruption event in the Earth’s plasma sheet [14]. In this paper we investigate magnetic field intermittence using q -th order moments (average of the powers) of wavelet coefficients. In the following under statistical moments we mean q -th order moments of wavelet coefficients. To be consistent, we specify the main problems related to the estimation of moments in the plasma sheet. First of all, a robust estimation of higher-order statistical characteristics of plasma sheet turbulence requires the processing of long time series, while the recited non-

steady features might change the internal structure of the observed turbulence. Contrarily, if the measurements are limited to too short time intervals, finite size effects lead to the divergence of higher order moments, and the description of fluctuations which show large deviations from a mean value becomes impossible. Additional difficulties are introduced by moment estimators which are not sensitive to the non-existence or divergence of statistical moments. Under the circumstances, for the proper recognition of the nature of large deviations in turbulence, at least three basic conditions have to be taken into account: 1.) the motion of PSBL, 2.) the time evolution of the driving and/or dissipation mechanisms and 3.) the number of existing statistical moments. One can detect PSBL motion (e.g. plasma sheet thinning or thickening) from direct, preferably multi-spacecraft observations [15, 16]. The driving and dissipation mechanisms are obviously dependent on the physical process examined. In this paper we analyse bursty bulk flow (BBF) associated magnetic fluctuations. Sporadically occurring BBFs can stir the plasma sheet plasma very efficiently, because they are the carriers of decisive amounts of mass, momentum and magnetic flux [17, 18]. Here the driver is the plasma flow itself, while the increased small scale power of the magnetic fluctuations can be used for a proper detection of ongoing dissipation processes. Then a statistical wavelet-based test ensuring the existence of moments can enhance the reliability of the intermittence level estimations.

II. WAVELET METHODS

In this paper we will use wavelet methods for the estimation of the power of small scale magnetic fluctuations, c_f , and for the computation and existence test of statistical moments, as well.

It was shown in Ref. 19 that a semi-parametric wavelet technique, based on a fast pyramidal algorithm, allows unbiased estimations of the scaling parameters c_f and α in the scaling relation for power spectral density $P(f) \sim c_f f^{-\alpha}$, where c_f is a nonzero constant. The algorithm consists of several steps. First, a discrete wavelet transform of the time series $X(t)$ is performed over a dyadic grid $(scale, time) = (2^j, 2^j t)$ and $j, t \in \mathbf{N}$. Then, at each octave $j = \log_2 2^j$, the variance μ_j of the discrete wavelet coefficients $d_x(j, t)$ is computed

through:

$$\mu_j = \frac{1}{n_j} \sum_{t=1}^{n_j} d_x^2(j, t) \sim 2^{j\alpha} c_f \quad (1)$$

where n_j is the number of coefficients at octave j . Finally, from Equation (1) α and c_f can be estimated by constructing a plot of $y_j \equiv \log_2 \mu_j$ versus j (logscale diagram) and by using a weighted linear regression over the region (j_{min}, j_{max}) where y_j is assumed to be a straight line.

Generalizing Equation (1), for a class of multifractal processes, the so-called partition function can be introduced through the q -th order moments of the wavelet coefficients [19]:

$$\mu_j^q = \frac{1}{n_j} \sum_{t=1}^{n_j} d_x^q(j, t) \sim 2^{j(\zeta(q)+q/2)} \quad (2)$$

The partition function measures not only the scaling of the moments, but also the higher order dependencies of the wavelet coefficients. When $\zeta(q)$ is plotted against q together with 95% confidence intervals of the mean $\zeta(q)$ (multiscale diagram), self-similar (fractal) and multifractal processes can be distinguished [19]. A nonlinear $\zeta(q)$ is a signature of multifractal scaling and small scale intermittence. However, the wavelet estimator may yield finite values for μ_j^q even in situations when a q -th order moment does not exist or diverges. This can happen when the higher order dependencies of the estimator rather than the true scaling of the moments are observed over a range of scales. The bias introduced by the estimator may prevent us from discriminating between monofractal and multifractal processes, because of the false nonlinear dependence of $\zeta(q)$ on q . In order to deduce the proper support of the partition function, (q_{min}, q_{max}) , over which all the moments exist and are finite, a simple method based on characteristic functions was proposed [20]. Here we shortly summarize this method. The empirical characteristic function for the time series X_n ($n = 1, \dots, N$) is computed as $F(u) = N^{-1} \sum_n e^{iuX_n}$. It represents the Fourier transform of the probability distribution of X . It has been proven that F has as many continuous derivatives at $u = 0$ as the probability distribution of X has finite positive integer moments. The generalization of the local integer degree of differentiability to real-valued degrees of differentiability is possible using the concept of Hölder regularity. The Hölder regularity of F at the origin ($u = 0$) controls the number of existing real-valued moments while $q_{max} \leq 2$. Only an averaged regularity of F around the origin is ensured to exist for moments exceeding 2 [21]. It introduces limitations to the testing procedure of existing moments larger than 2. It is possible, however, even in this case to estimate the lower and upper limit for the largest

existing positive moment q_{max} [20]. Since the wavelet transform, using a wavelet ψ with vanishing moments M_ψ , is well suited for estimating the Hölder regularity [22], F is wavelet transformed, and only the wavelet coefficients at the origin $d_F(s, u = 0)$ are considered further. Here instead of j the notation s is used for describing the characteristic scales of F . The number of vanishing moments M_ψ allows us to cancel or decrease the effects of linear or polynomial trends and ensures that the wavelet details are well defined. This is because a wavelet with M_ψ vanishing moments is orthogonal to the polynomials of degree $M_\psi - 1$ and the wavelet transform acts as a multiscale differential operator of order M_ψ [22]. The Hölder regularity of a signal can be estimated by wavelets with vanishing moments exceeding that Hölder regularity by at least 1. Then the Hölder regularity of F can be estimated from the decay of the wavelet coefficients across the scales. It allows to estimate q_{max} from a linear regression of $\log_2 d_F(s, u = 0)$ versus s . The largest existing negative moment q_{min} can be estimated by applying the same procedure as above, but for the inverse variable X^{-1} [20]. Further difficulties arise with finding the proper scales s over which the Hölder regularity of F can be evaluated. We will demonstrate that three different scaling ranges of F appear. One of them reflects the scaling properties of the chosen wavelet, and therefore the observed scaling over that range is not related to the physical process itself. This scaling range can be easily identified by changing the basic feature of the analysing wavelet: the number of vanishing moments M_ψ . To this end an appropriate wavelet has to be chosen which allows changing M_ψ . In this paper we use m -th order derivatives of the Gaussian wavelet which have m vanishing moments. The remaining two scaling ranges reflect a symmetry property of the estimator. An exchange of the time series X by X^{-1} results in a mirroring of the scaling regimes with respect to the characteristic scale which separates the tail from the body of the underlying distribution function. This symmetry feature of the estimator allows us to obtain both q_{min} and q_{max} at once, evaluating only the scaling properties of the characteristic function for the time series X [20]. We will consider further details of this method later.

III. BBF ASSOCIATED MAGNETIC TURBULENCE ON JULY 30, 2002

A. Event overview

In this paper we analyse burst mode (67 Hz) magnetic data from the Cluster fluxgate magnetometer (FGM) [23] during the interval 1730-1900 UT on July 30, 2002, when the Cluster (C) spacecraft were at the GSM (Geocentric Solar Magnetospheric) position $(-16, -11, 2)R_E$. The GSM coordinate system will be used throughout the paper, in which the x axis is defined along the line connecting the center of the Sun to the center of the Earth. The origin is defined at the center of the Earth and is positive towards the Sun. Figure 1a shows the B_X component from C 1,3. From 1730 to 1740 UT both spacecraft are in the lobe ($B_X \sim 30$ nT). After 1740 UT the spacecraft approach the neutral sheet ($B_X \rightarrow 0$) where they remain until almost 1900 UT. The B_Z component from C1,3 is depicted in Figure 1b together with a dashed line at the top indicating the occurrence of intermittent groups of BBF events. During the first half of the interval the velocity of the plasma flow increases up to 1500 km/s (not shown). BBFs drive the magnetic fluctuations of both B_X and B_Z components and cause a clear dipolarization of the magnetic field (increase of B_Z) at the beginning. Figure 1c shows the time evolution of the power of the B_Z fluctuations, $c_f(B_Z)$, which is estimated through Equation 1, in the logscale diagram, at the scale $j = 4$ (~ 0.33 s). $c_f(B_Z)$ is estimated within sliding overlapping windows of width 61 s with a time shift 4 s. All the variations of $c_f(B_Z)$ are relative enhancements to the lobe values which are normalized to 1. In this way $c_f(B_Z)$ represents a way of quantifying the relative power of the fluctuations at a given scale. In the following we restrict our analysis to the subintervals A and B , depicted in Figure 1c. During interval A , $c_f(B_Z)$ fluctuates intermittently on both C1 and C3. The difference in B_X measured at the locations of C1 and 3 changes substantially, indicating spatial gradient lengths of the order of the distance between the spacecraft. C1 and C3 are in opposite hemispheres in a distance ~ 4000 km before 1800 UT. The vertical position to the current sheet allows to use C1, C3 magnetic observations for rough estimation of the influence of PSBL. At the beginning of the interval A , B_X decreases from ~ 20 nT to ~ 0 nT showing large fluctuations about the mean value. After 1752 UT the fluctuations achieve ~ -20 nT. Both the large fluctuations and the values close to $-20, +20$ nT indicate that the magnetic fluctuations during the interval A might

be influenced by the PSBL. From the decreasing gradients after 1800 UT, we deduce that, the plasma sheet gradually becomes thicker. Both spacecraft stay closer to the neutral sheet and the amplitude of fluctuations is also considerably smaller. Therefore, the influence of the PSBL on turbulence characteristics might be weaker during the interval B . We will compare the higher-order statistical characteristics during the two intervals using magnetic data from C3. However, before that, the proper support of the partition function (Eq. 2) has to be evaluated.

B. Scaling of the characteristic function

Figure 2 shows the scaling properties of F computed for the B_Z component on C3 during period A . The continuous line corresponds to the estimated dependence of d_F on s at the origin in the log-log plot. The dashed-dotted lines show different scaling regimes. The interpretation follows the way proposed in Ref. 20. The maximum variance of F is controlled by the maximum value of B_Z . When the analysing scales go below $s_{min} \sim 1/\max(B_Z)$, the characteristic function is oversampled in the vicinity of the origin. Below s_{min} , the regularity of the analysing wavelet is observed. Therefore it shows a scaling $\sim s^{M_\psi}$, which is different from the scaling of F . The maximum scale, s_{max} , which separates the tail from the body of the underlying distribution function, can be found experimentally. For the scales $s \gg s_{max}$ the same scaling is observed as would have been obtained, if we had analysed a random variable B_Z^{-1} instead of B_Z . Figure 2 shows that for $\log_2 s > -3$, d_F scales as $\sim s^{\rho^-}$, therefore for the negative moments $q_{min} = \rho^-$. Between the scales (s_{min}, s_{max}) , the characteristic function scales as s^{ρ^+} . The estimated values are $\rho^- \sim -1.0 \pm 0.1$ and $\rho^+ \sim 2.2 \pm 0.1$. For period B , $\rho^- \sim -1.0 \pm 0.1$ and $\rho^+ \sim 2.4 \pm 0.1$ (not shown). In both cases the scaling exponent ρ^+ is larger than 2. In such a case the conditions for existing moments can be formulated in terms of an averaged Hölder regularity of F at the origin. To be able to detect the lower and upper bounds for an unknown average regularity, the number of vanishing moments (M_ψ) of the analysing wavelet has to be successively increased. First a low regularity wavelet can be chosen, e.g. the second derivative of the Gaussian wavelet. When the scaling exponent ρ^+ is equal or larger than 2, as in our case above, we can increase M_ψ until ρ^+ will achieve M_ψ between the scales (s_{min}, s_{max}) . It has been shown that when $\rho^+ \sim M_\psi$ is obtained, $\rho^+ < q_{max} < \rho^+ + 1$ [20]. On this basis $\zeta(q)$ can be computed

over the support $(q_{min}, q_{max}) = (-1, 3)$. The same computations for the B_X component of the magnetic field also give $q_{min} \sim -1$. Because of the small separation between s_{min} and s_{max} , however, it is not so straightforward to estimate q_{max} for B_X . Our estimation based on linear regression for different M_q s is $q_{max} = 1.5 \pm 0.5$. In what follows, the support $(q_{min}, q_{max}) = (-1, 3)$ will be used for both B_X and B_Z , having in mind that the estimate of $\zeta(q, B_X)$ is less reliable for $q > 2$.

C. Scaling of the moments

The dependence of $\zeta(q)$ on $q \in (q_{min}, q_{max})$ for B_X and B_Z estimated over two different range of scales during interval A is depicted in Figure 3. The large time scales 0.67 – 5.4 s, correspond to spatial scales of 670 – 5400 km, assuming 1000 km/s plasma flow velocities. The smaller value is of the order of the proton gyroradius in the plasma sheet, while the larger value is limited by the length of the intervals chosen. These values represent the lower end of the scale range of the MHD regime in turbulence. Similarly, the small time scales 0.08 – 0.33 s correspond to spatial scales 80 – 330 km where non-MHD dissipation and damping processes are non-negligible [2]. For what follows we will use the subscripts 'ss' for small scales and 'ls' for large scales. Except for $\zeta_{ss}(q > 0.5, B_X)$, $\zeta(q)$ exhibits linear dependence in the multiscale diagram (Figure 3). $\zeta_{ss}(q, B_X)$ is close to that linear dependence within $q \in (-1, 0.5)$.

Figure 4 shows the scaling of moments during interval B. $\zeta_{ls}(q)$ remains approximately linear for both B_X and B_Z . In comparison with interval A, the small scale behavior is different, $\zeta_{ss}(q, B_X) \sim 0$ for each q . In this case, the partition function (Eq.2) does not represent the effects of intermittence adequately, because of the flat power spectrum with a spectral index $\alpha = \zeta_{ss}(q = 2, B_X) + 1 \sim 1$ [24]. In contrast, $\zeta_{ss}(q < 2, B_Z)$ follows the straight line $\zeta(q) = q/3$, which describes the scaling in homogeneous Kolmogorov model of turbulence. However, $\zeta_{ss}(q > 2, B_Z)$ becomes undistinguishable from the large scale scalings (within the confidence intervals). This behavior indicates a weak multifractality in small scale vertical fluctuations of the magnetic field. Here, two additional points have to be clarified. First, in this paper we used magnetic field time series, therefore, when interpreting the observed scalings in terms of turbulence models, we have to suppose the validity of the Taylor frozen field hypothesis. In the plasma sheet the Taylor hypothesis is expected to be

valid during fast BBFs [25]. In our case plasma flow velocities achieve ~ 1500 km/s during the chosen intervals and the validity of the frozen field hypothesis seems to be substantiated. Second, instead of the velocity measurements, which are used in phenomenological models of hydrodynamic turbulence, we have magnetic field measurements, therefore the interpretation of $\zeta_{ss}(q, B_Z)$ in terms of Kolmogorov scaling might be difficult. Kolmogorov turbulence is completely described by its velocity field. If a passive scalar field is subject to Kolmogorov turbulence, the resulting scaling of the passive scalar field is also Kolmogorov [26]. The small scale weak magnetic field in the plasma sheet can be moved as a passive scalar and its scaling then resembles that of the velocity field. During the chosen intervals A and B, the small scale magnitude of the fluctuating magnetic field is a few nT, while the small scale velocity fluctuations achieve 500 km/s.

The significant difference between $\zeta_{ss}(q, B_X)$ and $\zeta_{ss}(q, B_Z)$ indicates that the small scale fluctuations appear to be anisotropic. To check this we plotted the time evolution of the relative power $c_{fr} = c_f(B_Z)/c_f(B_X)$ at scales 0.08 s and 5.4 s in Figure 5. c_{fr} was computed in the same way as c_f in Figure 1, using sliding overlapping windows. While the large scale (5.4 s) relative power of the B_Z and B_X fluctuations is close to one during the intervals A and B, the small scale (0.08 s) relative power shows significant enhancements. It means that magnetic fluctuations are excited preferentially in vertical direction during the intervals A and B. Outside of A and B the small scale power of the B_X and B_Z fluctuations is comparable. Large scale magnetic fluctuations exhibit more power in B_X than B_Z also outside the intervals A and B. These features show that the observed anisotropy is scale dependent and the occurrence of BBFs can modify the preferable direction of fluctuations.

In summary, the main difference between the intervals A and B is that small-scale magnetic fluctuations are less homogeneous during the interval B. Turbulence characteristics were expected to be influenced by the PSBL in A. Here the magnetic fluctuations can be more homogeneous due to an effective mixing of the plasma. The mixing length (ML) in the turbulent plasma sheet can be computed as the product of the integral time scale and the average root-mean-square velocity of turbulent flows, giving $ML \sim 10000$ km [1]. ML is of the order of the average distance that turbulent eddies can travel before colliding with each other. In Prandtl's mixing length theory [27] an effective viscosity is introduced which is proportional to ML^2 multiplied by the absolute value of the local velocity gradient. The velocity gradients are of the same order during A and B (not shown). However, ML

is position dependent. For turbulence close to a boundary, ML rapidly decreases, which makes the mixing of plasma more effective. Since the plasma sheet is thinner in A and thicker in B, ML should be shorter in A than in B. Nevertheless, the large scale scaling exhibits the same homogeneity in both A and B. The spectral index can be estimated as [24] $\alpha_{ls} = \zeta_{ls}(q = 2) + 1 \sim 2.7 \pm 0.7$. Similar values were obtained in Ref. 5. Interestingly, in wall-bounded turbulent shear flows $\alpha \sim 1.6 - 2.2$ is found [28]. We think that the longer ML led to the observed small scale anisotropy and weak multifractality during the interval B.

IV. CONCLUSIONS

Much of our recent knowledge about solar wind turbulence comes from both spectral and non-Gaussian (higher order statistical) properties of multiscale fluctuations. It is well understandable, since the available range of MHD scales of fluctuations in the solar wind embraces more than six decades of wave number space. In contrast, the range of available MHD scales in the plasma sheet spans over less than two decades [2]. In solar wind studies, depending on the length of the time series, moments (q -th order structure functions) up to $q = 20$ were computed [8]. Similar studies were not accomplished for plasma sheet turbulence.

In this paper we demonstrated that a proper study of the turbulence in the plasma sheet requires a thorough knowledge of the underlying non-steady physical conditions which can strongly influence the estimation of the turbulence characteristics. We studied BBF-associated magnetic fluctuations under conditions that allowed to consider the changing plasma sheet thickness and finite size effects. Using unsupervised methods, finite size effects can lead to spurious estimations of the scaling characteristics in turbulence. A possible solution of this problem comes from the study of the scaling features of the empirical characteristic function at the origin. We have shown that, at least for the analysed events, statistical moments can at best be computed for $q \in (-1, 3)$. So, the range of the available statistical moments is significantly different from that in the solar wind.

In spite of the restricted range, we have found that when the plasma sheet is thinner (Interval A), boundary effects lead to the shortening of the mixing length. The plasma is mixed more efficiently, and the small scale fluctuations become more homogeneous. The large

scale magnetic fluctuations are not sensitive to the changes of the plasma sheet thickness. Both BBF-associated intervals exhibit the same large scale scaling characteristics in the multiscale diagram similar to wall-bounded turbulent shear flows.

We have shown that non-homogeneous magnetic turbulence and a weak multifractality (nonlinear dependence of $\zeta(q)$ on q in multiscale diagram) develops in the vertical direction at small scales (0.08-0.33 s), when the fluctuations occur in a thick plasma sheet (Interval B), far from the PSBL. Though the multifractal signatures are indicative of an inhomogeneous energy transfer through a turbulent cascade, a model of intermittent turbulence (e.g. the P-model) cannot be fitted to the nonlinear $\zeta(q)$, because in such a model $\zeta(q = 3) = 1$ is expected [29]. In our case, however, $\zeta(q = 3) \gg 1$.

BBF associated magnetic fluctuations exhibit multi-scale anisotropy features which are different from non-BBF periods. The small scale scaling characteristics of B_X and B_Z fluctuations have found to be anisotropic in the multiscale diagrams. The occurrence of scale dependent anisotropy is evident from the comparison of the relative power of B_Z and B_X magnetic field fluctuations over two different scales (0.08 and 5.4 s). Scale dependent anisotropy can robustly appear in MHD fluids in the presence of a local mean magnetic field [4], but other mechanisms, e.g. velocity shears can also produce strong anisotropies [30].

A wider statistical study is needed, however, to explore fully the influence of the PSBL on magnetic turbulence and the appearance of anisotropy in the plasma sheet.

Acknowledgments

We thank H.-U. Eichelberger for help with FGM data.

-
- [1] J. E. Borovsky, R. C. Elphic, H. O. Funsten, and M. F. Thomsen, *J. Plasma Phys.* **57**, 1 (1997).
- [2] J. E. Borovsky and H. O. Funsten, *J. Geophys. Res.* **108**, 1284 (2003).
- [3] U. Frisch, *Turbulence* (Cambridge Univ. Press, Cambridge, 1995).
- [4] D. Biskamp, *Magnetohydrodynamic turbulence* (Cambridge Univ. Press, Cambridge, 2003).
- [5] M. Volwerk, W. Baumjohann, K.-H. Glassmeier, et al., *Compressional waves in the neutral sheet*, accepted for publication in *Ann. Geophys.*
- [6] Z. Voros, W. Baumjohann, R. Nakamura, et al., *Ann. Geophys.* **21**, 1955 (2003).
- [7] C. Pagel and A. Balogh, *Nonlin. Proc. Geophys.* **8**, 313 (2001).
- [8] E. Marsch and C. Y. Tu, *Nonlin. Proc. Geophys.* **4**, 101 (1997).
- [9] L. Sorriso-Valvo, V. Carbone, and P. Veltri, *Geophys. Res. Lett.* **26**, 1801 (1999).
- [10] E. Marsch and C. Y. Tu, *Ann. Geophys.* **12**, 1127 (1994).
- [11] Z. Voros, D. Jankovicova, and P. Kovacs, *Nonlin. Proc. Geophys.* **9**, 149 (2002).
- [12] P. Kovacs, V. Carbone, and Z. Voros, *Planet. Space. Sci.* **49**, 1219 (2001).
- [13] G. Consolini and T. Chang, *J. Atmosph. Sol. Terr. Phys.* **64**, 541 (2002).
- [14] A. T. Y. Lui and A. H. Najmi, *Geophys. Res. Lett.* **24**, 3157 (1997).
- [15] R. Nakamura, W. Baumjohann, H. Noda, et al., *Plasma sheet expansion observed by cluster and geotail*, accepted for publication in *Cosp. Coll. Ser.*
- [16] R. Nakamura, W. Baumjohann, T. Nagai, et al., *Flow shear near the boundary of the plasma sheet observed by cluster and geotail*, submitted to *J. Geophys. Res.*
- [17] V. Angelopoulos, W. Baumjohann, W. Kennel, et al., *J. Geophys. Res.* **97**, 4027 (1992).
- [18] R. Schodel, W. Baumjohann, R. Nakamura, V. A. Sergeev, and T. Mukai, *J. Geophys. Res.* **106**, 301 (2001).
- [19] P. Abry, P. Flandrin, M. S. Taqqu, and D. Veitch, *In. Self-similar network traffic and performance evaluation* (Wiley Interscience, New York, 2000), p. 39.
- [20] P. Goncalves and R. Riedi, *Diverging moments and parameter estimation*, submitted to *J. Am. Stat. Assoc.*
- [21] T. Kawata, *Fourier analysis in probability theory* (Academic Press, New York, 1972).
- [22] S. Mallat, *A wavelet tour of signal processing* (Academic Press, San Diego, 1999).

- [23] A. Balogh, C. M. Carr, M. H. Acuna, et al., *Ann. Geophys.* **19**, 1207 (2001).
- [24] C. Y. Tu, E. Marsch, and H. Rosenbauer, *Ann. Geophys.* **14**, 270 (1996).
- [25] T. S. Horbury, in *ESA Cluster II Worksh.* (2000), p. 89.
- [26] J. Cho, A. Lazarian, and E. T. Vishniac, *Lect. Notes Phys.* **614**, 56 (2003).
- [27] L. D. Landau and E. M. Lifshitz, *Fluid mechanics* (Pergamon Press, Oxford, 1987).
- [28] A. V. Johansson and P. H. Alfredsson, *J. Fluid Mech.* **137**, 409 (1983).
- [29] C. Pagel and A. Balogh, *J. Geophys. Res.* **107**, SSH 6 (2002).
- [30] M. S. Ruderman, M. L. Goldstein, D. A. Roberts, et al., *J. Geophys. Res.* **104**, 17057 (1999).

Figure captions

FIG. 1: Magnetic field measurements on Cluster 1 and 3; a. B_X components; b. B_Z components; c. Small scale power of B_Z fluctuations.

FIG. 2: Scaling of the characteristic function (continuous line); the observed scaling regimes (dashed-dotted lines); the exponent ρ^+ corresponds to the number of positive moments, ρ^- corresponds to the number of negative moments.

FIG. 3: Multiscale diagram - scaling of the moments is depicted for B_X and B_Z components at two different scale ranges within the interval A.

FIG. 4: Multiscale diagram - scaling of the moments is depicted for B_X and B_Z components at two different scale ranges within the interval B.

FIG. 5: Scale dependent anisotropy visible in time evolution of the relative power $c_{fr} = c_f(B_Z)/c_f(B_X)$.

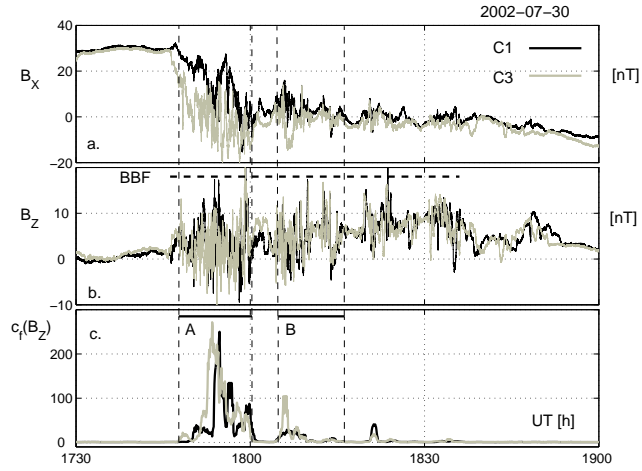


FIG. 1:

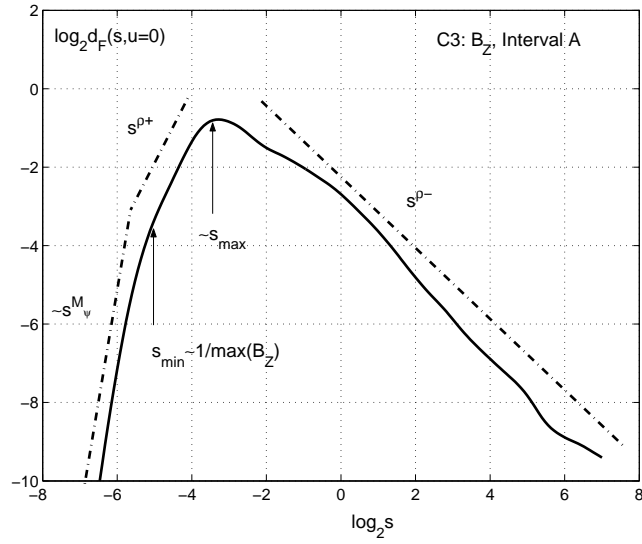


FIG. 2:

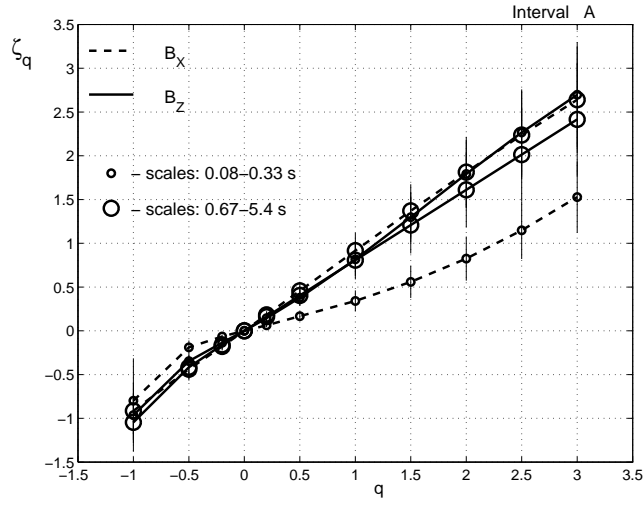


FIG. 3:

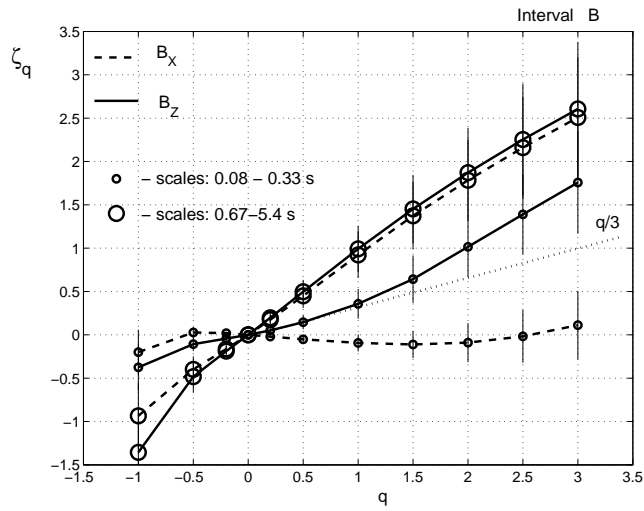


FIG. 4:

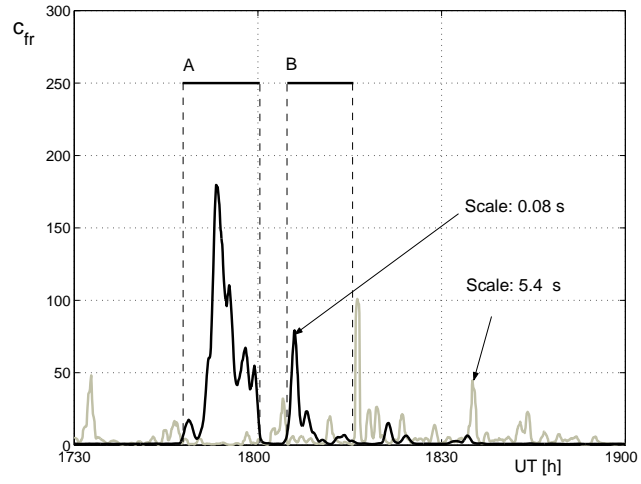


FIG. 5: